Computer Physics Communications 254 (2020) 107340

Contents lists available at ScienceDirect

Computer Physics Communications

journal homepage: www.elsevier.com/locate/cpc

SIDES: Nucleon–nucleus elastic scattering code for nonlocal potential☆,☆☆

G. Blanchon [a,*], M. Dupuis [a], H.F. Arellano [b,a], R.N. Bernard [c], B. Morillon [a]

[a] CEA,DAM, DIF F-91297 Arpajon, France
[b] Department of Physics - FCFM, University of Chile, Av. Blanco Encalada 2008, Santiago, Chile
[c] Department of Theoretical Physics, Research School of Physics, The Australian National University, Canberra, ACT 2601, Australia

ARTICLE INFO

Article history:
Received 28 October 2019
Received in revised form 6 March 2020
Accepted 5 April 2020
Available online 28 April 2020

Keywords:
Elastic scattering
Nonlocal potential

ABSTRACT

We introduce the package SIDES (Schrödinger Integro-Differential Equation Solver) that solves the integro-differential Schrödinger equation for elastic scattering of a nonlocal optical potential in coordinate space. The code is capable of treating the Coulomb interaction without restrictions. The method is based on previous developments by Jacques Raynal in the DWBA07 code. Elastic scattering observables such as differential and integral cross sections, as well as analyzing power and spin rotation functions for both neutron and proton projectiles are evaluated, with no restriction on the type of nonlocality of the potential nor on the beam energy. The corresponding distorted wavefunctions are calculated as well. The SIDES package includes a Perey–Buck potential generator with two parametrizations. It includes as well local potential parametrizations and allows for mixing local and nonlocal contributions. Benchmarks are performed and discussed.

Program summary

Program Title: SIDES
Program Files doi: http://dx.doi.org/10.17632/cmpjgyrngr.1
Licensing provisions: GNU General Public License, Version 2
Programming language: FORTRAN-90
Nature of problem: The description of nucleon elastic scattering off a target nucleus involves solving the Schrödinger's wave equation for positive incident energy. The determination of scattering observables calls for accurate treatments of the continuum. The effective coupling between the projectile and the target is accounted for by an optical potential, an operator which is by nature complex, energy-dependent and nonlocal. The coupling becomes long-range in the case of charged projectiles. In a general scenario under nonlocal potentials, Schrödinger's equation becomes an integro-differential equation.
Solution method: SIDES solves the Schrödinger integro-differential equation numerically by matrix inversion using Gibbs, Numerov or a modified Numerov method with a uniform radial mesh in a box. The solution is refined by an iterative procedure until a specified precision is achieved. To obtain elastic scattering observables, the associated phase-shifts are calculated *via* matching of the numerical solution with its analytic asymptotic behavior.

1. Introduction

Optical potentials are widely used to model nucleon elastic scattering off nuclei. These potentials are nonlocal, energy dependent and complex by nature, satisfying a dispersion relation related to causality. For convenience sake, local representations of optical potentials are often used but they lead to severe inconsistencies in the interpretation of experimental data regarding, for example, occupation numbers and matter densities as reported in Ref. [1]. Recently in the nuclear physics community, there has been a renewal of interest for nonlocal phenomenological [1–4] potentials based on energy density functionals [5–7], G-matrix-based [8,9] as well as *ab-initio* [10–12] optical potentials. The accurate treatment of nonlocality becomes crucial in order to reach a consistent description of nuclear structure and reactions. In the case of a nonlocal coupling between projectile and

☆ The review of this paper was arranged by Prof. Z. Was.
☆☆ This paper and its associated computer program are available via the Computer Physics Communication homepage on ScienceDirect (http://www.sciencedirect.com/science/journal/00104655).
* Corresponding author.
E-mail address: guillaume.blanchon@cea.fr (G. Blanchon).

https://doi.org/10.1016/j.cpc.2020.107340
0010-4655/

target, Schrödinger equation for scattering turns into an integro-differential equation in coordinate space. Here we present a dedicated code named SIDES that solves nucleon–nucleus scattering for any finite-range nonlocal complex potential, without resorting to any *ad-hoc* seed as required in iterative methods [4,13].

The acronym SIDES stands for Schrödinger Integro-Differential Equation Solver. This code stems from selected parts of the DWBA07 code developed by Jacques Raynal, where the author provides an accurate method to solve the Schrödinger equation under nonlocal potentials [14]. Among various tasks, the DWBA07 code was designed to calculate optical model potentials starting from local effective nucleon–nucleon interactions based on Hamburg and Melbourne g-matrices [15], resulting into nonlocal optical potentials. This specific scope, together with its sophisticated structure, impede its direct use to solve scattering from any external optical potential. To workaround this drawback, in this work we introduce a dedicated tool to solve the scattering problem under any kind of nonlocal potential. The wavefunction is obtained numerically by matrix inversion starting from one of the three proposed methods: Gibbs, Numerov or modified Numerov. Then scattering amplitudes are obtained by matching the numerical solution for the wavefunction with its asymptotic expression known analytically. Elastic scattering observables such as differential and integral cross sections, analyzing powers, and spin-rotation functions are computed, together with the corresponding distorted scattering waves.

Diverse methods of solution to Schrödinger's integro–differential equation can be found in the literature. Many of them follow iterative procedures [4,13,16], where a differential equation is integrated with a non-homogeneous term consisting of the projection of the nonlocal potential onto an intermediate solution. These procedures start with a given seed to generate the starting non-homogeneous term and implied intermediate solution. The new solution is subsequently fed back to construct a new non-homogeneous term, procedure which is interrupted once self-consistency is achieved. The efficacity of iterative methods may rely on prior knowledge of the solution, although there is no guarantee to converge to the actual solution. In the case of Ref. [17], a mean-value technique is applied to approximate projection of the non-local potential onto the scattering wave, reducing the problem to a second-order homogeneous differential equation.

More recently another approach has been proposed to deal with nonlocal potentials [18], where a Taylor approximation for the radial wave function is applied. This strategy is based on the assumption that nonlocality is dominant around the diagonal in coordinate space, feature observed in Perey–Buck nonlocal potentials but with limited validity. Indeed, in Ref. [19] it has been shown that microscopic potentials based on off-shell g matrices may exhibit sharp and oscillatory structure in coordinate space, features which call for robust techniques to solve the scattering problem.

An alternative method to obtain scattering waves in the presence of nonlocal potentials superposed to the long–range Coulomb interaction has been presented in Refs. [20,21], where Lanczos technique is applied to solve integral equations derived from the nonlocal Schrödinger equation. In Refs. [10,22,23] a numerical treatment to this problem has been introduced with the use of Berggren basis expansion, where an off-diagonal approximation is carried out to control the Coulomb singularity along the diagonal in momentum space. This method is well suited for medium excitation energies, of tens of MeV, and targets can be heavy nuclei. The Lagrange mesh method to calculate scattering states, reviewed in Ref. [24], is also widely used. A coordinate-space method to solve integro-differential equations in the context of the non-local Schrödinger equation has been presented in Ref. [25], where an iterative framework is considered for the calculation of complex-energy states. Note that these different methods are complementary: coordinate-space methods are the most precise, but can be unstable, especially if they are iterative. Methods based on Berggren basis expansion and Lagrange mesh, on the contrary, are very robust and can solve multi-channel problems, but precision, even if sufficient for practical purposes, is usually not as high as with coordinate-space methods.

Studies of the scattering problem of charged particles from nonlocal potentials have also been carried out in momentum space [26–32]. See Ref. [33] for a comprehensive review on the subject. While a clear advantage of momentum–space approaches is that nonlocalities are naturally accounted for, one of its shortcomings is that there is no method to obtain the scattering waves. When Coulomb interaction is suppressed the calculation of scattering amplitudes in momentum space is straightforward, reducing the problem to a Lippmann–Schwinger integral equation for the scattering matrix. However, in the presence of Coulomb potential the approach cannot be applied right away due to the $\sim 1/q^2$ singularity of the interaction. An exact solution addressing this singularity has been proposed by Vincent and Phatak by means of a cut-off technique to the Coulomb long-range tail [34]. This technique has been applied to proton–nucleus scattering at intermediate energies [27], including accurate multipole treatment of the charge form factor convoluted with a sharp cut-off potential [35].

Very recently a new technique has been introduced to solve the scattering problem under nonlocal potentials [36]. In the approach the Coulomb interaction is included and treated exactly. The method enables exact solutions for the scattering waves under nonlocal potentials in the presence of long-range Coulomb forces. The scattering process is described in the context of the Lippmann–Schwinger integral equation for the wavefunction, with the scattering waves obtained by direct matrix inversion. The robustness of this approach serves us as benchmark for solutions obtained from SIDES.

This article is organized as follows. In Section 2, after a brief introduction of the scattering formalism off a nonlocal potential, we layout the method to obtain the scattering amplitudes and their relationship with different observables of interest. Then in Section 3, we present in some detail the numerical method used in SIDES. In Section 4, we review the several local and nonlocal potential implemented in SIDES. The implementation of this package is then validated through a series of benchmarks discussed in Section 5, including applications for proton scattering from lead at beam energies up to 1 GeV. In Section 6, we give practical information on installation and operation of the code.

2. Nucleon–nucleus scattering with a nonlocal potential

For the sake of completeness, we layout some key elements of scattering theory needed to obtain elastic scattering observables in the context of nonlocal optical potentials. In this study we restrict ourselves to the scattering of spin–$\frac{1}{2}$ projectile from spin-0 target nuclei.

2.1. Integro-differential Schrödinger equation

Let us consider a projectile of mass M_p, spin $\frac{1}{2}$ and charge Z_p scattered off a spherical target of mass M_t, spin 0 and charge Z_t. The time-independent Schrödinger equation reads

$$-\frac{\hbar^2}{2\mu}\nabla^2\psi_{\mathbf{k}}(\mathbf{r})+V_C(\mathbf{r})\psi_{\mathbf{k}}(\mathbf{r})+\int U(\mathbf{r},\mathbf{r}';E)\psi_{\mathbf{k}}(\mathbf{r}')\mathrm{d}\mathbf{r}'=E\psi_{\mathbf{k}}(\mathbf{r}), \quad (1)$$

with E the projectile–target kinetic energy in the center of mass (c.m.), k the corresponding relative momentum and μ the

nucleon–nucleus reduced mass. The effective interaction between the nucleon and the nucleus consists of a non-local optical potential U. In the case of a charged projectile, the local potential V_C accounts for the Coulomb interaction due to the distributed charge in the target. Considering a closed-shell target the following partial-wave expansion for the scattering wavefunction becomes suitable [37],

$$\psi_{\mathbf{k}}(\mathbf{r}) = \sqrt{\frac{2}{\pi}} \sum_{jlm} i^l \mathcal{Y}^m_{jl1/2}(\hat{\mathbf{r}}) \frac{f_{lj}(k,r)}{kr} \mathcal{Z}^{jm*}_{l1/2\nu}(\hat{\mathbf{k}}). \tag{2}$$

In this expansion, $\mathcal{Y}$ and $\mathcal{Z}$ are defined as

$$\mathcal{Y}^m_{lj1/2}(\hat{\mathbf{r}}) = [Y_l(\hat{\mathbf{r}}) \otimes \chi_{1/2}]_{jm}, \tag{3}$$

$$\mathcal{Z}^{jm}_{l1/2\nu}(\hat{\mathbf{k}}) = \sum_{m_l=-l}^{+l} \langle lm_l, 1/2\nu | jm\rangle \, Y_l^{m_l}(\hat{\mathbf{k}}), \tag{4}$$

with $Y_l^{m_l}$ the spherical harmonic for orbital angular momentum l and projection m_l coupled to the spin function χ_s^σ. Furthermore, j represents total angular momentum. We can now replace $\psi_{\mathbf{k}}(\mathbf{r})$ from Eq. (2) in Eq. (1) in order to obtain the integro-differential Schrödinger equation for the radial wavefunction f_{lj}, namely

$$-\frac{\hbar^2}{2\mu}\left[\frac{d^2}{dr^2} - \frac{l(l+1)}{r^2}\right] f_{lj}(k,r) + V_C(r) f_{lj}(k,r) + r\int_0^\infty v_{lj}(r,r';E) f_{lj}(k,r') r' \mathrm{d}r' = E f_{lj}(k,r), \tag{5}$$

where the multipoles v_{lj} of the interaction are obtained from

$$v_{lj}(r,r';E) = \iint \mathrm{d}\hat{\mathbf{r}}\mathrm{d}\hat{\mathbf{r}}' \mathcal{Y}^{m\dagger}_{lj1/2}(\hat{\mathbf{r}}') U(\mathbf{r},\mathbf{r}';E) \mathcal{Y}^m_{lj1/2}(\hat{\mathbf{r}}). \tag{6}$$

We can recast the above equation for f_{lj} as

$$\frac{d^2}{dr^2} f_{lj}(r) + \int_0^\infty \mathcal{M}_{lj}(r,r';E) f_{lj}(k,r') \mathrm{d}r' = 0, \tag{7}$$

with

$$\mathcal{M}_{lj}(r,r';E) = \left(k^2 - \frac{l(l+1)}{r^2} - \frac{2\mu}{\hbar^2} V_C(r)\right)\delta(r-r') - \frac{2\mu}{\hbar^2} r r' v_{lj}(r,r';E). \tag{8}$$

In the particular case of local potentials, where U can be expressed as

$$U(\mathbf{r},\mathbf{r}';E) = V(\mathbf{r};E)\delta(\mathbf{r}-\mathbf{r}'), \tag{9}$$

Eq. (5) becomes the usual second-order differential equation for the wavefunction.

Applications at high incident energies require the account for relativistic effects. Corrections of kinematical origin are included as follows. Denoting with E_{lab} the kinetic energy of the projectile in the laboratory reference frame, then the projectile–target relative momentum k in the center-of-momentum reference frame is obtained from

$$k^2 = \frac{1}{4s}\left[s - (M_p + M_t)^2\right]\left[s - (M_p - M_t)^2\right], \tag{10}$$

where the s-invariant is given by $s = 2M_t E_{lab} + (M_p + M_t)^2$. These formulas are expressed in natural units $\hbar = c = 1$, for simplicity. Additionally, the reduced mass μ takes the form of the reduced energy

$$\mu \to \frac{E_p E_t}{E_p + E_t}, \tag{11}$$

with $E_p = \sqrt{k^2 + M_p^2}$, and $E_t = \sqrt{k^2 + M_t^2}$. The kinetic energy in the center-of-momentum reference frame is given by $E = E_p + E_t - M_p - M_t$.

2.2. Matching condition

For a finite-range nonlocal potential, the boundary between the inner radial region and the asymptotic one is set by imposing

$$v_{lj}(r,r';E) = 0\,, \quad \text{for } \min(r,r') \geqslant R. \tag{12}$$

In order to get the scattering wavefunction f_{lj} in the inner region, where the projectile remains sensitive to the finite range part of the optical potential (nuclear and finite range Coulomb contributions, including nonlocal Coulomb exchange), we solve Eq. (5) following the numerical method to be discussed in Section 3. In the asymptotic region the only coupling between the projectile and the charged nucleus is the point-Coulomb term given by

$$V_C(r) \underset{r\gtrsim R}{=} \frac{1}{4\pi\epsilon_0}\frac{Z_p Z_t e^2}{r}. \tag{13}$$

Under this regime the outgoing scattering waves take the analytic form

$$f_{lj}(k,r) \underset{r\gtrsim R}{=} \frac{i}{2}\left[H_l^{(-)}(kr) - S_l^j H_l^{(+)}(kr)\right], \tag{14}$$

where the S-matrix reads $S_l^j = \exp(2i\Delta_{lj})$. The $i/2$ factor is introduced in Eq. (14) to recover unperturbed (plane) waves in Eq. (2) when the interaction is set off, where $S_l^j = 1$. In the above expression $H_l^{(\pm)}$ are defined as

$$H_l^{(\pm)}(kr) = \exp(\mp i\sigma_l)\left[G_l(kr) \pm iF_l(kr)\right], \tag{15}$$

with F_l (G_l) the regular (irregular) spherical Coulomb function, under the phase convention that $F_0(x) = \sin(x)$, and $G_0(x) = \cos(x)$, when Coulomb contribution is off. The total phase-shift,

$$\Delta_{lj} = \sigma_l + \delta_{lj}, \tag{16}$$

consists of the Coulomb phase-shift σ_l and the short-range contribution δ_{lj}. Coulomb phase-shifts due to point sources are obtained analytically from the recursion relation

$$\sigma_{l+1} = \sigma_l + \mathrm{Arctg}\left(\frac{\eta}{l}\right) \tag{17}$$

with $\sigma_0 = \Gamma(1+i\eta)$, where $\eta = \mu Z_p Z_t e^2/\hbar^2 k$, is the Sommerfeld parameter [37,38]. The inner part of the wavefunction $f_{lj}^N(k,r)$ is obtained numerically following Section 3, where the resulting solution needs to be scaled in the form

$$f_{lj}(k,r) = \gamma_{lj} f_{lj}^N(k,r), \tag{18}$$

to match the asymptotic condition of Eq. (14). The coefficients S_l^j and γ_{lj} are obtained considering the solution of Eq. (14) at two radial points $r_\pm \equiv R \pm h$. Denoting

$$f_{lj}^\pm = f_{lj}^N(k,r_\pm), \quad F_l^\pm = F_l(kr_\pm) \quad \text{and} \quad G_l^\pm = G_l(kr_\pm), \tag{19}$$

then using Eqs. (14), (15) and (18), we get

$$\gamma_{lj} f_{lj}^\pm = \frac{i}{2}\exp(i\sigma_l)\Big[(1 - S_l^j\exp(-i2\sigma_l))G_l^\pm - i(1 + S_l^j\exp(-i2\sigma_l))F_l^\pm\Big]. \tag{20}$$

Finally we obtain for the $S-$matrix and the normalization coefficient γ_{lj},

$$S_l^j = \exp(2i\sigma_l)\frac{A_{lj} - iB_{lj}}{A_{lj} + iB_{lj}} \quad \text{and} \quad \gamma_{lj} = \exp(i\sigma_l)\left(A_{lj} + iB_{lj}\right)^{-1}, \tag{21}$$

where

$$A_{lj} = \frac{f_{lj}^+ G_l^- - f_{lj}^- G_l^+}{F_l^+ G_l^- - F_l^- G_l^+} \quad \text{and} \quad B_{lj} = \frac{f_{lj}^+ F_l^- - f_{lj}^- F_l^+}{F_l^+ G_l^- - F_l^- G_l^+}. \tag{22}$$

2.3. Elastic scattering observables

For spin $\frac{1}{2}$ - spin 0 particle scattering in the case of an unpolarized incident beam, the differential cross section reads

$$\frac{d\sigma}{d\Omega}(\theta) = |g(\theta)|^2 + |h(\theta)|^2, \tag{23}$$

where $g(\theta)$ ($h(\theta)$) is the scattering amplitude associated to particles with spin projection left unchanged (inverted) after scattering [38]. These amplitudes read

$$g(\theta) = f_c(\theta) + \frac{i}{2k}\sum_{l=0}^{\infty} e^{2i\sigma_l}\left\{(l+1)(1-S_l^{l+1/2}) + l(1-S_l^{l-1/2})\right\} P_l(\cos\theta),$$

$$h(\theta) = \frac{1}{2k}\sum_{l=0}^{\infty} e^{2i\sigma_l}\left\{(1-S_l^{l-1/2}) - (1-S_l^{l+1/2})\right\} P_l^1(\cos\theta). \tag{24}$$

Here $P_l(z)$ denotes the Legendre polynomial, and

$$P_l^n(z) = (-1)^n(1-x^2)^{n/2}\frac{d^n P_l(z)}{dz^n}, \tag{25}$$

the associated Legendre function. The Coulomb amplitude is given by

$$f_c(\theta) = \frac{-\eta}{2k\sin^2\left(\frac{\theta}{2}\right)}\exp\left[-i\eta\ \ln\left(\sin^2\left(\frac{\theta}{2}\right)\right) + 2i\sigma_0\right]. \tag{26}$$

With these definitions the corresponding integral cross sections read

$$\sigma_R = \frac{\pi}{k^2}\sum_{l=0}^{\infty}\left\{(l+1)\left(1-\left|S_l^{l+1/2}\right|^2\right) + l\left(1-\left|S_l^{l-1/2}\right|^2\right)\right\}, \tag{27}$$

$$\sigma_{SE} = \frac{\pi}{k^2}\sum_{l=0}^{\infty}\left\{(l+1)\left|1-S_l^{l+1/2}\right|^2 + l\ \left|1-S_l^{l-1/2}\right|^2\right\}, \tag{28}$$

$$\sigma_T = \frac{\pi}{k^2}\sum_{l=0}^{\infty}\left\{(l+1)\left[1-\mathrm{Re}(S_l^{l+1/2})\right] + l\ \left[1-\mathrm{Re}(S_l^{l-1/2})\right]\right\}. \tag{29}$$

Here σ_R, σ_{SE} and σ_T denote reaction, shape elastic and total cross sections, respectively.

The presence of spin–orbit coupling affects the spin orientation of the projectile through the collision process. A measure of this effect is given by the analyzing power, which reads

$$A_y(\theta) = \frac{2\ \mathrm{Re}\left[g^*(\theta)h(\theta)\right]}{|g(\theta)|^2 + |h(\theta)|^2}. \tag{30}$$

Being an interference effect, A_y vanishes if one of the amplitudes, g or h, is equal to zero. The analyzing power also vanishes if one amplitude is real and the other one is pure imaginary [38]. Another spin observable is the spin rotation, commonly denoted by Q, given by the ratio

$$Q(\theta) = \frac{2\ \mathrm{Im}\left[g^*(\theta)h(\theta)\right]}{|g(\theta)|^2 + |h(\theta)|^2}. \tag{31}$$

Results for differential elastic observables are given in terms of θ and corresponding momentum transfer given by $q = 2k\sin(\theta/2)$.

3. Numerical method of solution

We present the numerical method we adopt to solve Eq. (5) and obtain the radial wavefunctions f_{lj}^N in a radial box of size R defined in Eq. (12). As already mentioned in Eq. (18), the numerical wavefunction is then scaled through the matching procedure. Thus, one wants to solve

$$\frac{d^2}{dr^2}f_{lj}(r) + \int_0^R \mathcal{M}_{lj}(r,r';E)f_{lj}(r')\mathrm{d}r' = 0, \tag{32}$$

with conditions at the border. From now on, subscripts referring to angular momentum and energy are omitted for simplicity, as Eq. (32) is solved independently for each (l,j) pair. Eq. (32) is discretized over a uniform radial mesh of size R and step h, with

$$\begin{aligned} dr' &\longrightarrow h \\ r &\longrightarrow ih \\ r' &\longrightarrow jh \\ f(r) &\longrightarrow f_i \\ \mathcal{M}(r,r';E)dr' &\longrightarrow M_{i,j} \end{aligned}$$

with indices i and j ranging from 0 to N. The use of trapezoidal rule in Eq. (32) yields

$$f_i'' + \sum_{j=0}^{N} M_{i,j}f_j = 0. \tag{33}$$

We present and examine three methods to solve Eq. (33), namely Gibbs, Numerov, and the modified Numerov methods.

3.1. Gibbs' method

The above equation can be solved using numerical differentiation method for the second derivative and matrix inversion as described by Gibbs [39]. We refer to this method as Gibbs' method for convenience. The second derivative is obtained using a three-point differentiation formula

$$f_i'' = \frac{f_{i+1} - 2f_i + f_{i-1}}{h^2} + \mathcal{O}(h^2). \tag{34}$$

Replacing this expression in Eq. (33) yields

$$\left[\boldsymbol{B} + h^2\boldsymbol{M}\right]\boldsymbol{f} = 0, \tag{35}$$

where $\boldsymbol{B}$ is a tri-diagonal matrix whose elements are given by

$$B_{i,j} = (\delta_{i,j-1} - 2\delta_{i,j} + \delta_{i,j+1}), \tag{36}$$

with $1 \le i \le N$. The problem is reduced to a system of N equations corresponding to $r = h, 2h, \ldots, Nh$. Since we have $N+2$ unknowns $(f_0, f_1, \ldots, f_{N+1})$, the system is algebraically underdetermined. However, from a physics standpoint we impose $f_0 = 0$, in order to ensure regularity of the solution at the origin. Additionally we can impose

$$f_{N+1} \equiv 1, \tag{37}$$

which is equivalent to choose an arbitrary normalization of the wave function. Considering that the short-range potential is negligible above the matching radius, we have $M_{i,N+1} = 0$ for $i = 1, \ldots, N$. The only element in Eq. (36) containing f_{N+1} comes from the term $\delta_{N,N+1}$, which once placed as an inhomogeneous term in the same system leads to

$$\sum_{j=1}^{N}\mathcal{K}_{i,j}f_j = b_i, \tag{38}$$

with $b_i = 0$, for $i < N$, and $b_N = -f_{N+1}$. Matrix $\mathcal{K}$ in Eq. (38) is defined as

$$\mathcal{K}_{i,j} = \left[(\delta_{i,j+1} - 2\delta_{i,j} + \delta_{i,j-1}) + h^2 M_{i,j}\right] - \delta_{i,N}\delta_{j,N+1}. \tag{39}$$

The solution of Eq. (38) is obtained after inverting the complex matrix $\mathcal{K}$,

$$f_i = -\left(\mathcal{K}^{-1}\right)_{i,N} \quad \text{for} \quad i \in [1,N], \quad f_0 = 0 \quad \text{and} \quad f_{N+1} = 1. \tag{40}$$

The matching procedure described in the previous Section is then used to get the phase-shift and the normalization of the wave function.

3.2. Numerov method

An alternative approach to solve Eq. (32) comes from the use of Numerov's technique to solve a second-order differential equations. This method [14,40,41] allows better control in the precision of second derivatives, where

$$(f_{i+1} - 2f_i + f_{i-1}) = \frac{h^2}{12}(f''_{i+1} + 10f''_i + f''_{i-1}) + \mathcal{O}(h^6). \tag{41}$$

Then, Eq. (41) can be recast as

$$\xi_{i+1} - 2\xi_i + \xi_{i-1} = u_i, \tag{42}$$

where each element ξ_i of vector $\boldsymbol{\xi}$ is defined as

$$\xi_i = f_i - \frac{1}{12}u_i, \tag{43}$$

and

$$u_i = h^2 f''_i. \tag{44}$$

Eq. (42) can then be written in a matrix form,

$$\boldsymbol{B}\boldsymbol{\xi} = \boldsymbol{u} \tag{45}$$

with $\boldsymbol{B}$ defined in Eq. (36). After combining Eqs. (33), (43), (44) and (45), we get

$$\left[\boldsymbol{B} + h^2\boldsymbol{M}\left(\frac{1}{12}\boldsymbol{B} + \boldsymbol{1}\right)\right]\boldsymbol{\xi} = 0. \tag{46}$$

Finally, we obtain

$$\sum_{j=1}^{N}\left[(\delta_{i,j+1} - 2\delta_{i,j} + \delta_{i,j-1}) + \frac{h^2}{12}(M_{i,j+1} + 10M_{i,j} + M_{i,j-1})\right] \xi_j = 0, \tag{47}$$

for $i = 1, \ldots, N$. We then proceed in the same way as in the Gibbs' method. We have now

$$\sum_{j=1}^{N}\mathcal{K}_{i,j}\xi_j = b_i, \tag{48}$$

with $b_i = 0$, for $i < N$, and $b_N = -\xi_{N+1}$. We impose $\xi_{N+1} \equiv 1$ and define

$$\mathcal{K}_{i,j} = \left[(\delta_{i,j+1} - 2\delta_{i,j} + \delta_{i,j-1}) + \frac{h^2}{12}(M_{i,j+1} + 10M_{i,j} + M_{i,j-1})\right] - \delta_{i,N}\delta_{j,N+1}. \tag{49}$$

The solution of Eq. (48) is obtained after inverting the complex matrix $\mathcal{K}$,

$$\xi_i = -\left(\mathcal{K}^{-1}\right)_{i,N} \quad \text{for} \quad i \in [1, N], \quad \xi_0 = 0 \quad \text{and} \quad \xi_{N+1} = 1. \tag{50}$$

The wave function $\boldsymbol{f}$ can be obtained from $\boldsymbol{\xi}$ using relations

$$f_i = \xi_i + \frac{1}{12}u_i \tag{51}$$

$$= \frac{1}{12}\left[\xi_{i-1} + 10\xi_i + \xi_{i+1}\right] \tag{52}$$

3.3. Modified Numerov method

We now consider a Modified Numerov Method (MNM) that results to be more accurate than the two previous approaches. Jacques Raynal is referred to as inventor of the method in Ref. [42]. MNM has also been used in the context of coupled-channel calculations with local optical potentials, where the computation of the solution involves the resolution of a linear system of equation [43]. We start again from Eq. (42) with

$$\boldsymbol{u} = \frac{h^2\boldsymbol{M}}{1 - \frac{h^2}{12}\boldsymbol{M}}\boldsymbol{\xi}. \tag{53}$$

The modified Numerov method consists in expanding the fraction in the expression of $\boldsymbol{u}$ up to fourth order in h,

$$\boldsymbol{u} \approx \left\{h^2\boldsymbol{M} + \frac{h^4}{12}\boldsymbol{M}^2\right\}\boldsymbol{\xi}\,. \tag{54}$$

Then, Eq. (53) can be written as Eq. (48). Considering the boundary conditions for $\boldsymbol{\xi}$, we get the solution by matrix inversion in the same way as described previously. The error induced by the truncated development in Eq. (54) is of the same order than the one yielded by Numerov method except for its sign. This results in a compensatory effect between the two sources of error as described in more detail in Ref. [43].

3.4. Refinement procedure

We have presented three methods to obtain the solution of Eq. (33), each of them with a different truncation error. Moreover, they are based on a numerical inversion of matrix $\mathcal{K}$, procedure that induces numerical errors. We now show a method aimed to refine the numerical accuracy of the result, an issue which has been discussed in detail in Ref. [44].

Let us recast Eq. (33) such as

$$\boldsymbol{\mathcal{A}}\boldsymbol{f} = \boldsymbol{b}\,, \tag{55}$$

where $\boldsymbol{\mathcal{A}}$ has a truncation error lower than $\mathcal{K}$ and $\boldsymbol{b}$ takes care of the boundary conditions. Denote with $\mathcal{N}$ the inverse of $\mathcal{K}$ obtained numerically. We now define the $\boldsymbol{R}$ matrix with

$$\boldsymbol{R} = \boldsymbol{1} - \boldsymbol{\mathcal{N}}\boldsymbol{\mathcal{A}}\,. \tag{56}$$

Thus $\boldsymbol{R}$ measures the accuracy by which $\mathcal{N}$ is the true inverse of $\boldsymbol{\mathcal{A}}$. Combining Eqs. (55) and (56) we obtain

$$\boldsymbol{f} = \boldsymbol{\mathcal{N}}\boldsymbol{b} + \boldsymbol{R}\boldsymbol{f}\,. \tag{57}$$

Assuming that the coefficients of $\boldsymbol{R}$ are strictly smaller than 1, then the above Eq. (57) yields for the exact solution $\boldsymbol{f} = (\boldsymbol{1} + \boldsymbol{R} + \boldsymbol{R}^2 + \cdots)\boldsymbol{\mathcal{N}}\boldsymbol{b}$. With this result in mind it becomes useful to define

$$\boldsymbol{f}^{(n)} = (\boldsymbol{1} + \boldsymbol{R} + \cdots + \boldsymbol{R}^n)\,\boldsymbol{\mathcal{N}}\,\boldsymbol{b}\,. \tag{58}$$

Thus, defining $\boldsymbol{f}^{(0)} = \boldsymbol{\mathcal{N}}\boldsymbol{b}$, then for $n > 0$ we have

$$\boldsymbol{f}^{(n)} = \boldsymbol{f}^{(n-1)} + \boldsymbol{R}^n\,\boldsymbol{\mathcal{N}}\boldsymbol{b}\,. \tag{59}$$

With this construction, the exact solution $\boldsymbol{f}$ is given by $\boldsymbol{f}^{(\infty)}$. In practice, we proceed recursively until the difference between two consecutive orders is small enough under a given criteria. In our case we define

$$S^{(n)} = \sum_{i=1}^{N}|\delta f_i^{(n)}|^2\,, \tag{60}$$

where

$$\delta\boldsymbol{f}^{(n)} \equiv \boldsymbol{R}^n\,\boldsymbol{\mathcal{N}}\boldsymbol{b} = \boldsymbol{R}\,\delta\boldsymbol{f}^{(n-1)}\,. \tag{61}$$

With the above, the condition for convergence is defined as

$$S^{(n)} \leq \epsilon\,. \tag{62}$$

To achieve this condition it is essential to calculate $\delta\boldsymbol{f}^{(n)}$ with higher precision than the original solution of Eq. (40). To this purpose we pay special attention to the precision of the numerical differentiation used for second derivatives when determining $\boldsymbol{\mathcal{A}}$.

Table 1
Nonlocal optical model parameters for neutrons for the Perey–Buck potential from Ref. [13]. The depth parameters are in MeV units, while geometry parameters are in fm units.

	U_v	r_v^R	a_v^R	W_s	r_s^I	a_s^I	U_{so}	r_{so}	a_{so}	β
Neutron	71.00	1.22	0.65	15.00	1.22	0.47	7.18	1.22	0.65	0.85

Table 2
Same as Table 1 for Tian, Pang and Ma potential from Ref. [3].

	U_v	r_v^R	a_v^R	W_v	r_v^I	a_v^I	W_s
Neutron	70.00	1.25	0.61	1.39	1.17	0.55	21.11
Proton	70.95	1.29	0.58	9.03	1.24	0.50	15.74
	r_s^I	a_s^I	U_{so}	r_{so}	a_{so}	β	r_C
Neutron	1.15	0.46	9.00	1.10	0.59	0.90	
Proton	1.20	0.45	8.13	1.02	0.59	0.88	1.34

Once the condition in Eq. (62) is fulfilled the system is considered as solved (default value $\epsilon = 10^{-6}$ fm^{-1}).

For the cases of Numerov and modified Numerov methods the refinement procedure differs slightly. There we start from an equation of the form,

$$\mathcal{K}\boldsymbol{\xi} = \boldsymbol{b}\,. \tag{63}$$

As previously $\mathcal{A}$ stands for the system bringing the desired solution $\boldsymbol{f}$ with a better precision than the first solution $\boldsymbol{\xi}^{(0)} = \mathcal{N}\boldsymbol{b}$. $\boldsymbol{\xi}^{(n)}$ is defined as in Eq. (58) with $\boldsymbol{\xi}$ instead of $\boldsymbol{f}$. Whenever coefficients of $\boldsymbol{R}$ are strictly smaller than 1, one gets $\boldsymbol{\xi}^{(\infty)} = \boldsymbol{f}$.

4. Potentials

SIDES can be used with any microscopic or phenomenological local and nonlocal potential in coordinate space through input file. Some parametrizations are provided as well.

4.1. Perey-Buck nonlocal potentials

This class of potential is build from Woods–Saxon form factors and Gaussian nonlocality. In addition, it includes local terms for the spin–orbit and Coulomb contributions. SIDES is shipped with the original Perey–Buck parametrization [13] fitted for neutron elastic scattering, together with a more recent parametrization developed for both neutron and proton projectiles by Tian, Pang and Ma (TPM) [3]. These two sets are energy independent, although both have been developed for maximum nucleon energy of about 30 MeV. Tables 1 and 2 summarize these two parametrizations. The routine `PEREY` can be used, for instance, as a starting point to generate nonlocal dispersive optical potentials from Refs. [1,45]. Moreover it can be easily modified to produce PB potential dependent on the incident energy as proposed in [46–48] or with different nonlocalities for each term. The routine performs partial-wave expansion as

4.2. Local potentials

The Koning–Delaroche (KD) global parametrization of the local optical potential is provided [49]. The global dispersive local optical potential from Morillon–Romain (MR) is provided as well [50]. Both potentials work for neutron and proton projectiles with energy from 1 keV to 200 MeV off (near-)spherical nuclides in the mass range $24 < A < 209$. The MR potential requires the knowledge of the target neutron and proton Fermi energies. We use the KD prescription for the Fermi energy. The user can easily modify the beginning of `pot_mr.f90` file in order to use a better prescription.

5. Benchmarks

In this Section, we evaluate the convergence ability of SIDES using the three methods outlined in Section 3, namely Gibbs, Numerov and modified Numerov method. We also assess the effectiveness of the refinement method described in Section 3.4. We first consider the case of a separable nonlocal potential solvable analytically. Then we perform some benchmarks comparing our results with the ones obtained with ESW from Ref. [36], using TPM potential as given by Table 2, and microscopic model potentials at high energies.

5.1. Comparison with an analytically solvable model

We compare scattering results from SIDES with exact solutions given by a separable potential. This assessment is made suppressing the Coulomb interaction. In this case we focus on the total cross section. Following Bagchi and Mulligan [51], we consider separable construction

$$v_{lj}(r, r') = \frac{1}{rr'} q(r) q(r'). \tag{64}$$

Then using

$$q(r) = Ae^{-\alpha r} r^n, \tag{65}$$

one obtains an analytical solution for the phase-shift. For the sake of simplicity, we consider a single partial wave $l = 0$ and $j = 1/2$. In the following, we refer to cross sections obtained analytically as 'Analytic Result' (AR). For $q(r)$ in Eq. (65) we adopt the following set of parameters with $A = 25\hbar^2/\mu$, μ the reduced mass in the case of neutron scattering off ^{40}Ca, $\alpha = 6.5$ and $n = 1$. In Fig. 1, we present results in a radial box of 10 fm, considering only the s-wave. We show results for several values of the number of radial steps $N = 50$, 100 and 200. In both Figures, frames (a), (b) and (c) correspond to Gibbs' approach; frames (d), (e) and (f) to Numerov's approach; and frames (g), (h) and (i) to MNM. Frames in the first column correspond to the total cross section σ_0 as a function of the energy, while the second column represents the corresponding error relative to AR. In these three cases the refinement procedure has been applied. Frames in the third column show results without the refinement of the solution. Only converged results are depicted. One notices that for a given value of N, Numerov and MNM converge far better than Gibbs' method. Moreover in the second column, errors beyond 10% are not depicted for sake of clarity. As a result, we can safely state that the Modified Numerov Method can be safely used checking the convergence with the radial step and with L_{max}.

5.2. Convergence with the mesh size

We now illustrate the convergence of the solution as a function of the density of mesh points in the radial box, specified by N. In this case we focus on the total cross section σ_T for $n+^{40}$Ca elastic scattering, and the reaction cross section σ_R for $p+^{40}$Ca. The projectile kinetic energy is 30.3 MeV, with the use of TPM potential (see Section 4) to represent the interaction between the projectile and the nucleus. The size of the radial box is $R = 15$ fm, considering $l \leq 20$. Let N be the dimension of the radial array, and denote with $\sigma^{(N)}$ its resulting cross section. As a measure of convergence, let us define $D_N = |1 - \sigma_T^{(N)}/\sigma_T^{(NF)}|$, with NF a sufficiently large number for which convergence is acceptable. With this definition, small values of D_N indicate proximity of the solution to the acceptable one.

In frames (a) and (b) of Fig. 2 we plot $\log(D_N)$ for neutron scattering as a function of N, for $20 \leq N \leq 180$, with $NF = 200$. These frames correspond to results using Numerov method

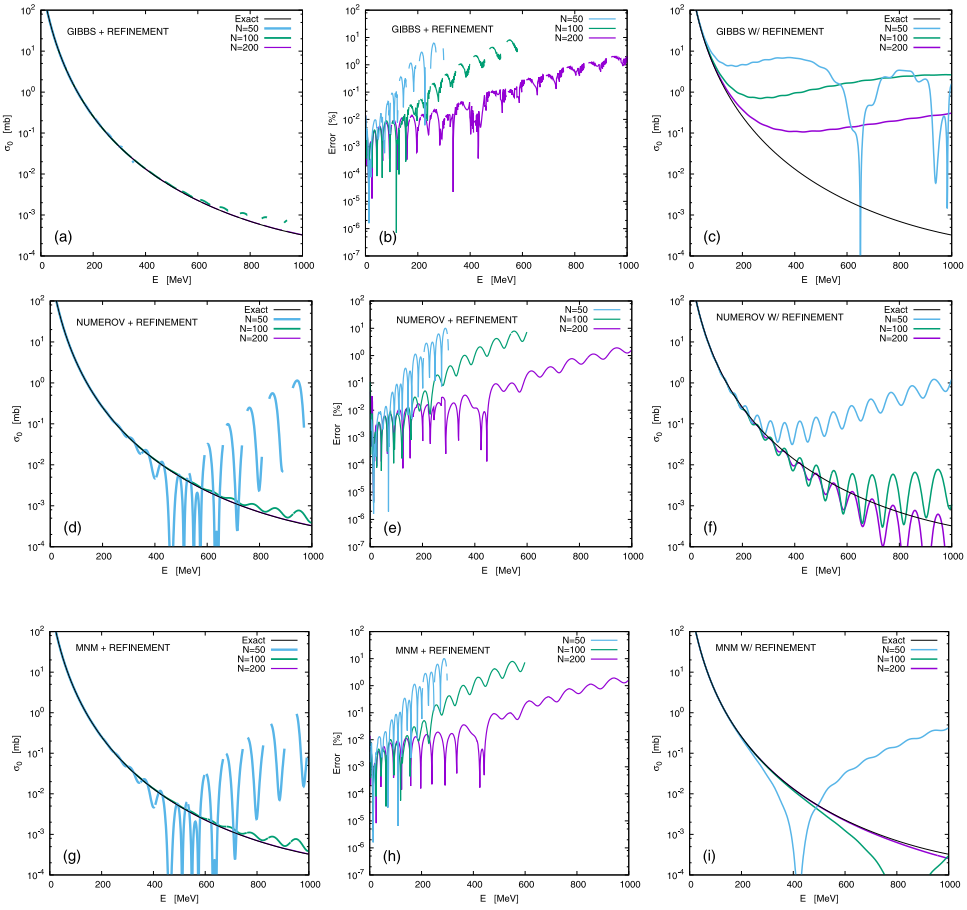

Fig. 1. Convergence tests for the *s*-wave elastic cross section as function of the incident energy. Results are obtained with the three proposed methods: Gibbs (panels a, b and c), Numerov (panels d, e and f), and modified Numerov (panels g, h and i). The refinement procedure is (not) used in the calculation when '(w/) correction' is mentioned. Black solid curves refer to AR solutions based on separable potential with parameter set 1. See text for explanation of each frame.

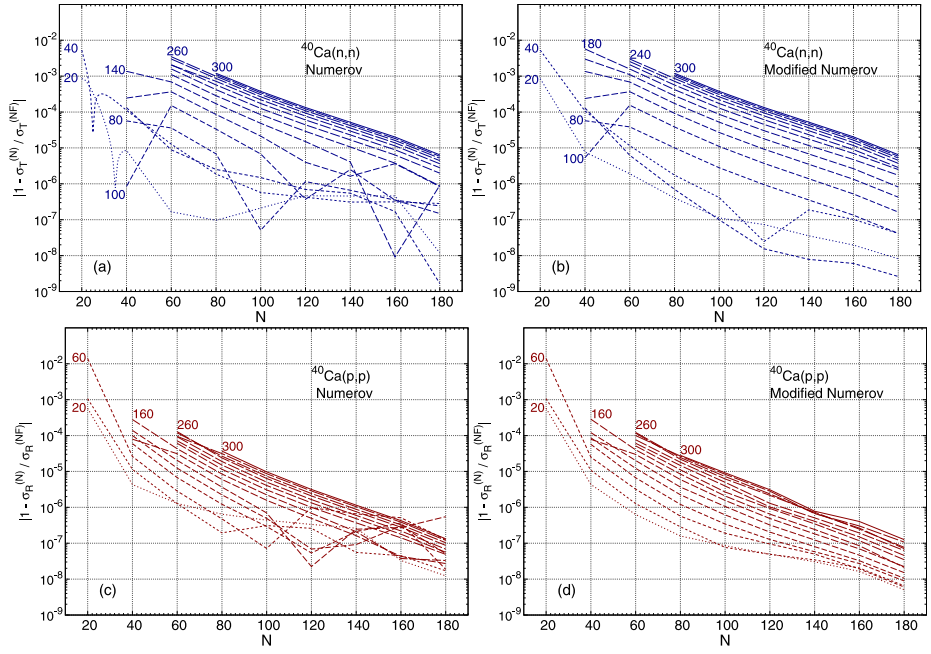

Fig. 2. Rate of convergence of calculated reaction (total) cross section for p (n)+^{40}Ca elastic scattering function of the dimension N of radial array for several incident energies indicated in MeV. The reference cross section, $\sigma^{(NF)}$ is taken with $N = 200$. Radial box of $R = 15$ fm. Calculation done with TPM potential.

and MNM, respectively. Labels on the curves correspond to the energy in MeV units. As observed, the result converges to the reference calculation with increasing N, as expected. Also, for a given proximity D_N, say 10^{-4} for instance, the needed N for such accuracy increases with the energy. In the case of 300 MeV, the needed N is $\sim$ 130, whereas for 100 MeV the needed N is $\sim$70. When comparing Numerov method with MNM, we observe that the latter converges more monotonically to the solution than Numerov alone.

Frames (c) and (d) show logarithmic plots for D_N based on reaction cross sections for proton scattering. In this case we also note a monotonic convergence to the solutions when MNM is applied, with proximity to the converged value below 10^{-6} when $N \geq 60$. Qualitative features in the convergence of the solutions are similar to the ones exhibited for the reaction cross sections.

5.3. Full calculation

We now analyze proton scattering off ^{40}Ca, comparing results from SIDES and the ones from the method reported in Ref. [36], to be labeled ESW (Exact Scattering Waves). The referred method leads to exact solutions for the scattering waves for nonlocal potentials in the presence of long-range Coulomb forces. The scattering process is described in the context of the Lippmann–Schwinger integral equation for the wavefunction, allowing to obtain the scattering waves by simple matrix inversion. In Fig. 3 we compare SIDES and ESW results for ^{40}Ca(p, p) scattering at 30 MeV, where we use TPM optical potential from Ref. [3]. Upper (a), middle (b) and lower (c) frames show the differential cross section $d\sigma/d\Omega$, analyzing power A_y and spin rotation Q, respectively. As observed, the differential cross section exhibits near complete agreement between the two approaches, with a slight difference at the minimum at scattering angles around 140°. In the case of the analyzing power, a difference in 0.2 appears in the last minimum. A similar difference takes place for the last two maxima in Q. Apart from these two differences, both spin observables are consistently calculated by these two approaches for scattering angles below 120°.

We include a calculation for proton elastic scattering off ^{208}Pb target at 500 MeV, 800 MeV and 1 GeV. For this application we construct optical potentials of '$t\rho$' type [27], where off-shell t matrices are obtained from Argonne v_{18} bare potential. The use of free t matrix at these high energies is justified by the fact that medium effects are weak. Additionally, the inclusion of inelasticities of nucleon–nucleon interactions is dealt with following Ref. [52]. The obtained effective interaction is then folded with matter density [53] obtained from Hartree–Fock–Bogoliubov with D1S Gogny interaction [54,55]. Results are shown in Fig. 4, where results from SIDES are compared with the results obtained with ESW [36]. SIDES results are obtained using the Numerov method, as results obtained with MNM are identical. All calculations are performed in a 15 fm box. We assess the convergence of the calculation varying the number of radial integration step taking $N = 150$ and $N = 300$. Differential cross sections are practically identical with both models and converged for both discretization. Analyzing powers and Q observables are globally in agreement between the two models even if they converge slower with N especially increasing momentum transfer q. These results demonstrate the ability of SIDES to handle accurately high energy processes as well. Moreover it is worth mentioning that SIDES is able to handle as input microscopic potentials with very exotic structures such as the ones presented in Ref. [19].

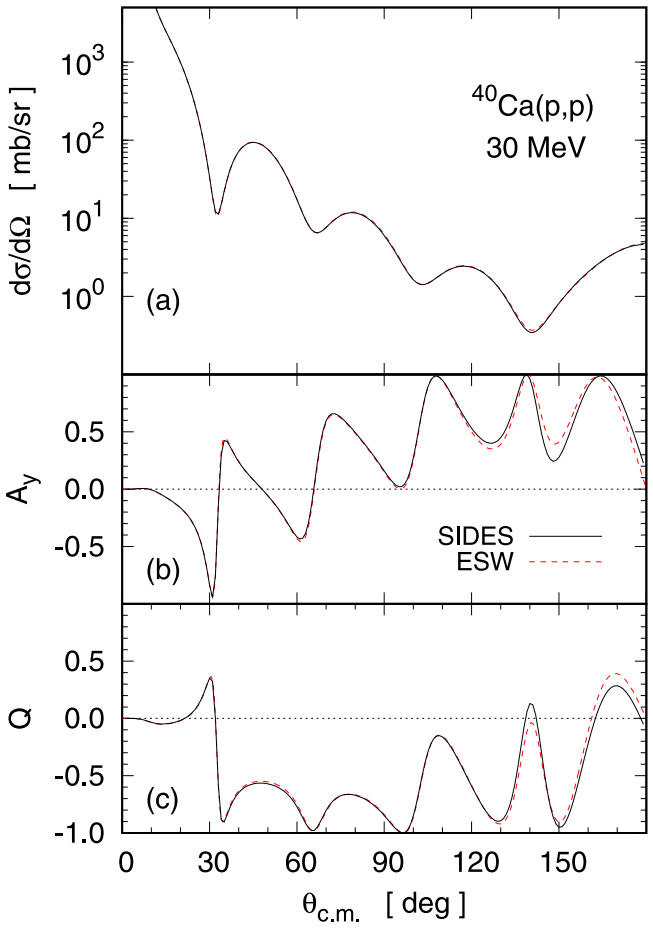

Fig. 3. Calculated differential cross section (a), analyzing power (b) and spin rotation (c) as functions of the center-of-mass scattering angle. TPM potential for ^{40}Ca(p, p) elastic scattering at 30.3 MeV is used [3]. Black (red) curves denote results from SIDES (ESW) [36]. (For interpretation of the references to color in this figure legend, the reader is referred to the web version of this article.)

6. Program SIDES

6.1. Compiling and running

The code package contains 22 subroutines and 2 functions written in Fortran 90. After downloading the source code SIDES.tar.gz, one should unzip the tar file:

```
gunzip SIDES.tar.gz
tar -xvf SIDES.tar
```

This will create the directory `SIDES/`. The package SIDES is composed of the following directories and files:

- `README`: contains detailed instructions to build the solver, the tools and their dependencies, and to run the code with the examples provided.
- `Makefile`: a standard GNU makefile to build the solver and the tools. The user can modify the compiler there.
- `src/`: Fortran source files for SIDES.
- `UNSAVE`: type `./UNSAVE` in order to move `file-SAVE` to `file`. Useful when the user wishes to use potentials previously stocked.

The full SIDES package is independent of any library.

The code is compiled typing in `src/`:

```
make
```

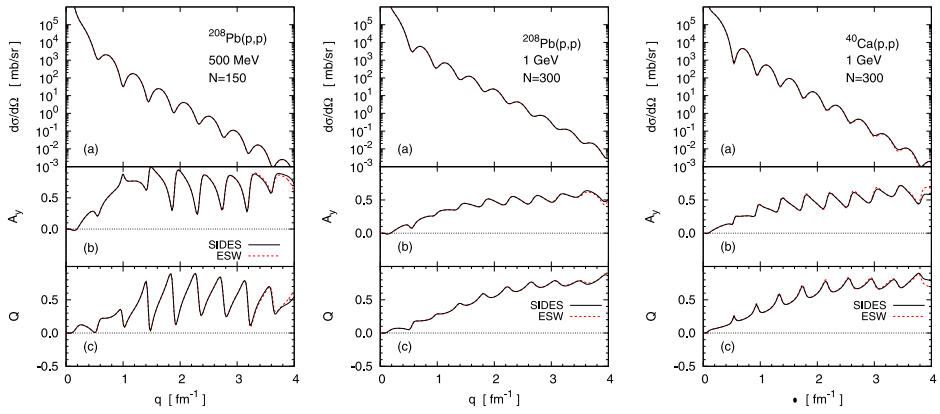

Fig. 4. Calculated differential cross section (a), analyzing power (b) and spin rotation (c) as functions of the center-of-mass scattering angle. ^{208}Pb(p,p) elastic scattering at 500 MeV and 1 GeV with potential from g matrix starting from bare interaction av18 [52]. Same for ^{40}Ca(p,p) at 1 GeV. Black (Red) curves denote results from SIDES (ESW) [36]. (For interpretation of the references to color in this figure legend, the reader is referred to the web version of this article.)

Table 3
Constants used in SIDES.

Conversion constant	$\hbar c = 197.3269788$ MeV fm
Fine-structure constant	$\alpha = \frac{e^2}{4\pi\epsilon_0\hbar c} = 1/137.035999$
Unified atomic mass unit	$M_u = 931.49432$ MeV/c^2
Neutron mass	$M_n = 1.008665$ u
Proton mass	$M_p = 1.007276$ u

The code can be run typing: `run` and then answering to the questions in the terminal. Using a given input the code is simply run typing

```
./SIDE < input
```

6.2. Constants & units

By default, the usual constants are set following Ref. [56]. Constants are stocked in the module `DEF_CONST` in files `def_const.f90`. Whenever the value of a constant is modified, the user has to go through (see Table 3).

```
make clean
make
```

6.3. Input files

In this Section, we present the input files required to run SIDES. Depending on the options, the following files are needed as input.

6.3.1. Input

After compilation, run the code doing `./sides < INPUT`. We now describe the inputs.

- `ZPROJ` *(integer)* projectile:
  - (0) neutron
  - (1) proton
- `TAR ATARGET ZTARGET` *(character*2, integer, integer)* target symbol, mass, charge.
- `IETEST` *(integer)* incident energy and maximum ℓ value:
  - (1) read from input `ENERGY LMAX` *(real*8, integer)*
  - (2) read from file `ENERGIES` located in the main directory
- `REL` *(integer)* kinematics:
  - (0) non relativistic
  - (1) relativistic
- `TYP` *(integer)* type of potential:
  - (1) local potential: `NCHOIX` *(integer)*:
    - (1) read from file `LOCPOTENTIAL` in main directory
    - (2) Köning-Delaroche global local potential
    - (3) Morillon-Romain global dispersive local potential
    - (4) custom potential with parameters set by the user in `potloc.f90`:
      `ICOU` *(integer)* Add a local uniformly charged sphere Coulomb potential: (0) no, (1) yes
  - (2) nonlocal potential `NCHOIX` *(integer)*:
    - (1) read from file `NLPOTENTIAL` in main directory
    - (2) Tian, Pang and Ma nonlocal potential potential
    - (3) Perey-Buck nonlocal potential (valid only for incident neutron)
    - (4) custom Perey-Buck-like potential with parameters set by the user in `perey.f90`
      `ICOU` *(integer)* Add a local uniformly charged sphere Coulomb potential: (0) no, (1) yes
  - (3) local+nonlocal potential:
    - `NCHOIXLOC` *(integer)*
      - (1) read from file `LOCPOTENTIAL` in main directory
      - (2) Köning-Delaroche global local potential
      - (3) Morillon-Romain global dispersive local potential
      - (4) custom potential with parameters set by the user in `potloc.f90`
        `ICOU` *(integer)* Add a local uniformly charged sphere Coulomb potential: (0) no, (1) yes
    - `NCHOIXNL` *(integer)*
      - (1) read from file `NLPOTENTIAL` in main directory
      - (2) Tian, Pang and Ma nonlocal potential potential
      - (3) Perey-Buck nonlocal potential (valid only for incident neutron)
      - (4) custom Perey-Buck-like potential with parameters set by the user in `perey.f90` (`ICOU` imposed to 0)
- `SAVEPOT` *(integer)*

(0) Potential not saved
(1) Potential saved on LOCPOTENTIAL and/or NLPOTENTIAL followed by an illuminating suffix i.e. LOCPOTENTIAL-pCa40_10.000-SAVE.

- METHOD *(integer)*

(1) Numerov
(2) Modified Numerov
(3) Gibbs

- IR *(integer)* Maximum radius

(1) defined by user RMAX *(real)*
(2) pre-defined value RMAX=15 fm

- NMAX *(integer)* Number of steps

(1) defined by user NMAX *(integer)*
(2) pre-defined value N=150

- IA *(integer)* Angular step number

(1) defined by user TTMAX *(integer)*
(2) pre-defined value TTMAX=179

6.3.2. Energies

This files is used when IETEST=2. Energies and corresponding maximum l values (see Eqs. (29)) should be provided as follows

```
ENERGY1  LMAX1
ENERGY2  LMAX2
...
```

SIDES is executed for each line of the file. LMAX required for convergence of the cross section increases with incident energy. The user is invited to check the convergence of the calculation using different values of LMAX.

6.3.3. Read local potential

For NCHOIX=1 and TYP=1 or 3, the local contribution to the potential is read in the main folder from the file LOCPOTENTIAL (ex: LOCPOTENTIAL-pCa40_20.000) in the following format:

```
ZPROJ  ATARGET  ZTARGET  ENERGY  STEP  NMAX  LMAX  ICOU
L  J
REAL PART  IMAGINARY PART
...
```

The first line of the file contains information suitable to identify the potential: projectile, target mass and charge, incident energy in the laboratory frame, radial step, number of radial steps, maximum l value. The consistency between the input parameters and the first line parameter is checked during the run. Multipoles are ordered as: $(l = 0, j = 1/2)$, $(l = 1, j = 1/2)$, $(l = 1, j = 3/2)$ and so on until $l =$ LMAX. For each (l, j)-value, the potential is read and symmetrized in the routine vr_reader.f90 using

```
DO K1=1,NMAX
READ(1,*) VX,VY
CV(K1,K1) = DCMPLX(VX,VY)
ENDDO
```

ICOU variable has to be set to 0 if Coulomb is already contained in the potential for proton scattering or in the case of neutron scattering. For ICOU=1 a uniformly charged sphere Coulomb potential is added to the potential. The value of R_c adopted is indicated during the run and is taken as $R_c = 1.34\, A^{1/3}$. Different prescriptions for Coulomb can be easily implemented modifying file vr_reader.f90.

6.3.4. Read nonlocal potential

For NCHOIX=1 and TYP=2 or 3, the nonlocal contribution to the potential is read in the main from the file NLPOTENTIAL (ex: NLPOTENTIAL-pCa40_20.000). The file contains the multipole expansion of the nonlocal potential $v_{lj}(r, r'; E)$ as described in Eq. (6). This file is organized in the same way than for local potentials. The potential is read and symmetrized in the routine vrrp_reader.f90 following,

```
DO K1=1,NMAX
  DO K2=1,K1  !<-- WARNING
    READ(1,*) VX,VY
    CV(K2,K1) = DCMPLX(VX,VY)
    CV(K1,K2) = CV(K2,K1)
  ENDDO
ENDDO
```

Please read the previous section in order to carefully address the choice if ICOU. Different prescriptions for Coulomb can be easily implemented modifying file vrrp_reader.f90.

6.4. Output files

We now present the different outputs of SIDES. Besides the information provided in the terminal during the run, SIDES provides several output files.

6.4.1. SIDES-...

The main output is of the type SIDES-pCa40-30.000-PB-NM-R for proton elastic scattering off ^{40}Ca at 30 MeV with Perey–Buck potential, Numerov method and relativistic kinematics. It contains a detailed record of input parameters. The different differential observables are proposed with center-of-mass scattering angle, momentum transfer (expressed at end of Section 2), differential cross section (Eq. (23)), differential cross section divided by Rutherford for proton scattering, analyzing power (Eq. (30)) and Q observable (Eq. (31)) as follows

```
## Angle  q  Cross section  C.S./Rutherford  Ay
Q
## [deg.] [1/fm] [mb/sr]
...
```

Then integral cross sections are printed: reaction, elastic and total cross section for neutron and only reaction cross section for proton.

It contains as well phase-shifts δ_{lj} (Eq. (16)).

```
#     PHASE-SHIFTS (LMAX= ...)
# L  Delta(j = l-1/2)  Delta(j = l+1/2)
#      [rad]           [rad]
...
```

This output file allows for straightforward plots of results using gnuplot.

6.4.2. INTEGRAL-CROSS-SECTION-...

Integral cross sections are provided separately as function of the incident energy. This is convenient when several energies are read from file.

6.4.3. DW-...

This file contains wavefunctions f_{lj} from Eq. (18). It is organized as follows

```
## Wavefunctions for n+40Ca elastic scattering @
40 MeV and LMAX=30
##     l j=l-1/2                  l j=l+1/2
r   Re[f_lj(r)]  Im[f_lj(r)]   Re[f_lj(r)]  Im[f_lj(r)]
...
```

6.4.4. LOCPOTENTIAL...-SAVE and/or NLPOTENTIAL...-SAVE

When POTSAVE=1 the total potential is saved in file, meaning the sum of nuclear and Coulomb contributions. The stocked potentials can then be used as input potentials provided the -SAVE suffix is suppressed. Typing ./UNSAVE allows for this change a

file name. The first line of the file indicates the main parameters of the calculation.

```
ZPROJ ATARGET ZTARGET ENERGY H NMAX LMAX ICOU
L J
...
```

ICOU is set by default to 0. This prevents from double counting of Coulomb when the potential will be used as input.

7. Summary and conclusions

We have presented the SIDES package capable of solving nucleon–nucleus elastic scattering under any kind of short-range nonlocal potential. The code has been designed to solve the integro-differential nonrelativistic Schrödinger equation for spin−0 target, including the long-range Coulomb interaction. Applications have been tested at beam energies of up to 1 GeV, leading to confident results for differential as well as integral cross sections, including analyzing power A_y and spin rotation function Q. Furthermore, SIDES provides results for the scattering distorted waves in (j, l) basis. For testing purposes, the package features a built-in Perey–Buck potential generator with two parametrizations. Some local parametrizations are provided as well in order to be used within the same package. It is as well possible to mix local and nonlocal contributions. In this paper, we have summarized the main theoretical considerations and numerical strategies in line with the actual implementation of the code. In particular, we discuss and include three alternative methods to handle finite-differences, with subsequent reduction of the integro-differential equation into matrix form. Furthermore, the refinement procedure aimed to correct truncation errors is presented and implemented in SIDES. This contribution represents the first self-contained computational code capable of solving Schrödinger's integro-differential equation, in its exact form, without feedback iterative methods nor resorting to the construction of alternative bases.

Declaration of competing interest

The authors declare that they have no known competing financial interests or personal relationships that could have appeared to influence the work reported in this paper.

Acknowledgments

G. B. and M. D. warmly thank Jacques Raynal for his help. G. B. thanks Pierre Chau for his help. H. F. A. wishes to thank to colleagues of CEA, DAM, DIF for their kind hospitality during his stay at Bruyères-le-Châtel, where part of his contribution to this collaboration took place.

References

[1] M.H. Mahzoon, R.J. Charity, W.H. Dickhoff, H. Dussan, S.J. Waldecker, Phys. Rev. Lett. 112 (2014) 162503.
[2] A. Ross, L.J. Titus, F.M. Nunes, M.H. Mahzoon, W.H. Dickhoff, R.J. Charity, Phys. Rev. C 92 (2015) 044607.
[3] Y. Tian, D.-Y. Pang, Z.-Y. Ma, Internat. J. Modern Phys. E 24 (01) (2015) 1550006, http://dx.doi.org/10.1142/S0218301315500068, URL https://www.worldscientific.com/doi/abs/10.1142/S0218301315500068.
[4] L. Titus, A. Ross, F. Nunes, Comput. Phys. Comm. 207 (2016) 499–517, http://dx.doi.org/10.1016/j.cpc.2016.06.022, URL http://www.sciencedirect.com/science/article/pii/S0010465516302028.
[5] K. Mizuyama, K. Ogata, Phys. Rev. C 86 (2012) 041603.
[6] T.V. Nhan Hao, B.M. Loc, N.H. Phuc, Phys. Rev. C 92 (2015) 014605.
[7] G. Blanchon, M. Dupuis, H.F. Arellano, N. Vinh Mau, Phys. Rev. C 91 (2015) 014612.
[8] H.F. Arellano, F.A. Brieva, W.G. Love, Phys. Rev. Lett. 63 (6) (1989) 605–608.
[9] M. Dupuis, S. Karataglidis, E. Bauge, J.P. Delaroche, D. Gogny, Phys. Rev. C 73 (1) (2006) 014605.
[10] J. Rotureau, P. Danielewicz, G. Hagen, F.M. Nunes, T. Papenbrock, Phys. Rev. C 95 (2017) 024315, http://dx.doi.org/10.1103/PhysRevC.95.024315, URL https://link.aps.org/doi/10.1103/PhysRevC.95.024315.
[11] A. Idini, C. Barbieri, P. Navrátil, J. Phys. Conf. Ser. 981 (1) (2018) 012005, URL http://stacks.iop.org/1742-6596/981/i=1/a=012005.
[12] M. Burrows, C. Elster, S.P. Weppner, K.D. Launey, P. Maris, A. Nogga, G. Popa, Phys. Rev. C 99 (2019) 044603, http://dx.doi.org/10.1103/PhysRevC.99.044603.
[13] F. Perey, B. Buck, Nuclear Phys. 32 (1962) 353–380.
[14] J. Raynal, Computer code DWBA07, 2007, (NEA 1209/08).
[15] K. Amos, P.J. Dortmans, H.V. von Geramb, K. S., R. J., Adv. Nucl. Phys. 25 (2000) 275.
[16] L.J. Titus, F.M. Nunes, Phys. Rev. C 89 (2014) 034609.
[17] N.J. Upadhyay, A. Bhagwat, B.K. Jain, J. Phys. G: Nucl. Part. Phys. 45 (1) (2018) 015106, URL http://stacks.iop.org/0954-3899/45/i=1/a=015106.
[18] N.J. Upadhyay, A. Bhagwat, Phys. Rev. C 98 (2018) 024605, http://dx.doi.org/10.1103/PhysRevC.98.024605, URL https://link.aps.org/doi/10.1103/PhysRevC.98.024605.
[19] H.F. Arellano, G. Blanchon, Phys. Rev. C 98 (2018) 054616, http://dx.doi.org/10.1103/PhysRevC.98.054616, URL https://link.aps.org/doi/10.1103/PhysRevC.98.054616.
[20] B.T. Kim, T. Udagawa, Phys. Rev. C 42 (1990) 1147–1149, http://dx.doi.org/10.1103/PhysRevC.42.1147, URL https://link.aps.org/doi/10.1103/PhysRevC.42.1147.
[21] B. Kim, M. Kyum, S. Hong, M. Park, T. Udagawa, Comput. Phys. Comm. 71 (1) (1992) 150–158, http://dx.doi.org/10.1016/0010-4655(92)90080-I, URL http://www.sciencedirect.com/science/article/pii/001046559290080I.
[22] G. Hagen, N. Michel, Phys. Rev. C 86 (2012) 021602.
[23] N. Michel, Phys. Rev. C 83 (2011) 034325, http://dx.doi.org/10.1103/PhysRevC.83.034325, URL https://link.aps.org/doi/10.1103/PhysRevC.83.034325.
[24] D. Baye, Phys. Rep. 565 (2015) 1–107, http://dx.doi.org/10.1016/j.physrep.2014.11.006, The Lagrange-mesh method. URL http://www.sciencedirect.com/science/article/pii/S0370157314004086.
[25] N. Michel, Eur. Phys. J. A 42 (3) (2009) 523, http://dx.doi.org/10.1140/epja/i2008-10738-7.
[26] A. Picklesimer, P.C. Tandy, R.M. Thaler, D.H. Wolfe, Phys. Rev. C 30 (1984) 1861–1879, http://dx.doi.org/10.1103/PhysRevC.30.1861, URL https://link.aps.org/doi/10.1103/PhysRevC.30.1861.
[27] H.F. Arellano, F.A. Brieva, W.G. Love, Phys. Rev. C 41 (1990) 2188–2201, http://dx.doi.org/10.1103/PhysRevC.41.2188.
[28] C. Elster, T. Cheon, E.F. Redish, P.C. Tandy, Phys. Rev. C 41 (3) (1990) 814–827.
[29] R. Crespo, R.C. Johnson, J.A. Tostevin, Phys. Rev. C 41 (5) (1990) 2257–2262.
[30] C.R. Chinn, C. Elster, R.M. Thaler, Phys. Rev. C 44 (1991) 1569–1580, http://dx.doi.org/10.1103/PhysRevC.44.1569, URL https://link.aps.org/doi/10.1103/PhysRevC.44.1569.
[31] D.H. Lu, T. Mefford, R.H. Landau, G. Song, Phys. Rev. C 50 (1994) 3037–3046, http://dx.doi.org/10.1103/PhysRevC.50.3037, URL https://link.aps.org/doi/10.1103/PhysRevC.50.3037.
[32] N.J. Upadhyay, V. Eremenko, L. Hlophe, F.M. Nunes, C. Elster, G. Arbanas, J.E. Escher, I.J. Thompson, Phys. Rev. C 90 (2014) 014615, http://dx.doi.org/10.1103/PhysRevC.90.014615, URL https://link.aps.org/doi/10.1103/PhysRevC.90.014615.
[33] L. Ray, G. Hoffmann, W. Coker, Phys. Rep. 212 (5) (1992) 223–328, http://dx.doi.org/10.1016/0370-1573(92)90156-T, URL http://www.sciencedirect.com/science/article/pii/037015739290156T.
[34] C.M. Vincent, S.C. Phatak, Phys. Rev. C 10 (1974) 391–394, http://dx.doi.org/10.1103/PhysRevC.10.391, URL https://link.aps.org/doi/10.1103/PhysRevC.10.391.
[35] R.A. Eisenstein, F. Tabakin, Phys. Rev. C 26 (1982) 1–7, http://dx.doi.org/10.1103/PhysRevC.26.1, URL https://link.aps.org/doi/10.1103/PhysRevC.26.1.
[36] H.F. Arellano, G. Blanchon, Phys. Lett. B 789 (2019) 256–261, http://dx.doi.org/10.1016/j.physletb.2018.12.004, URL http://www.sciencedirect.com/science/article/pii/S0370269318309274.
[37] C.J. Joachain, Quantum Collision Theory, North-Holland Publishing Company, Amsterdam, 1975.
[38] A.G. Sitenko, Scattering Theory, in: Springer Series in Nuclear and Particle Physics, Springer, 1991.

[39] W.R. Gibbs, Computation in Modern Physics, World Scientific Pub. Co. Inc., Singapore, 2006.
[40] P.H. Cowell, A.C.D. Crommelin, Greenwich Observations in Astronomy, Magnetism and Meteorology made at the Royal Observatory, Series 2, Vol. 71, 1911, pp. O1–O84.
[41] B.V. Noumerov, Mon. Not. R. Astron. Soc. 84 (8) (1924) 592–602, http://dx.doi.org/10.1093/mnras/84.8.592, arXiv:http://oup.prod.sis.lan/mnras/article-pdf/84/8/592/3661174/mnras84-0592.pdf.
[42] M. Melkanoff, T. Sawada, J. Raynal, Nuclear Optical Model Calculations, Numerical Analysis Research, Department of Engineering, Department of Physics, University of California, and the Department of Physics, University of Southern California, 1965, URL https://books.google.fr/books?id=ZXflygAACAAJ.
[43] J. Raynal, Computer code ecis03, 2004, (NEA 0850/16).
[44] W.H. Press, W.T. Vetterling, S.A. Teukolsky, B.P. Flannery, Numerical Recipes in C++: The Art of Scientific Computing, second ed., Cambridge University Press, New York, NY, USA, 2002, page 60.
[45] W.H. Dickhoff, R.J. Charity, M.H. Mahzoon, J. Phys. G: Nucl. Part. Phys., 44 (3) (2017) 033001, URL http://stacks.iop.org/0954-3899/44/i=3/a=033001.
[46] C. Engelbrecht, H. Fiedeldey, Ann. Physics 42 (2) (1967) 262–295, http://dx.doi.org/10.1016/0003-4916(67)90071-1, URL http://www.sciencedirect.com/science/article/pii/0003491667900711.
[47] A.E. Lovell, P.-L. Bacq, P. Capel, F.M. Nunes, L.J. Titus, Phys. Rev. C 96 (2017) 051601, http://dx.doi.org/10.1103/PhysRevC.96.051601, URL https://link.aps.org/doi/10.1103/PhysRevC.96.051601.
[48] M.I. Jaghoub, A.E. Lovell, F.M. Nunes, Phys. Rev. C 98 (2018) 024609, http://dx.doi.org/10.1103/PhysRevC.98.024609, URL https://link.aps.org/doi/10.1103/PhysRevC.98.024609.
[49] A.J. Koning, J.P. Delaroche, Nuclear Phys. A713 (3–4) (2003) 231–310.
[50] B. Morillon, P. Romain, Phys. Rev. C 76 (4) (2007) 044601.
[51] B. Bagchi, B. Mulligan, Phys. Rev. C 10 (1974) 126–135, http://dx.doi.org/10.1103/PhysRevC.10.126, URL https://link.aps.org/doi/10.1103/PhysRevC.10.126.
[52] H.F. Arellano, H.V. von Geramb, Phys. Rev. C 66 (2) (2002) 024602.
[53] H.F. Arellano, M. Girod, Phys. Rev. C 76 (2007) 034602, http://dx.doi.org/10.1103/PhysRevC.76.034602, URL https://link.aps.org/doi/10.1103/PhysRevC.76.034602.
[54] J. Dechargé, D. Gogny, Phys. Rev. C 21 (4) (1980) 1568–1593.
[55] J.F. Berger, M. Girod, D. Gogny, Comput. Phys. Comm. 63 (1991) 365.
[56] M. Tanabashi, K. Hagiwara, K. Hikasa, K. Nakamura, Y. Sumino, F. Takahashi, J. Tanaka, K. Agashe, G. Aielli, C. Amsler, M. Antonelli, D.M. Asner, H. Baer, S. Banerjee, R.M. Barnett, T. Basaglia, C.W. Bauer, J.J. Beatty, V.I. Belousov, J. Beringer, S. Bethke, A. Bettini, H. Bichsel, O. Biebel, K.M. Black, E. Blucher, O. Buchmuller, V. Burkert, M.A. Bychkov, R.N. Cahn, M. Carena, A. Ceccucci, A. Cerri, D. Chakraborty, M.-C. Chen, R.S. Chivukula, G. Cowan, O. Dahl, G. D'Ambrosio, T. Damour, D. de Florian, A. de Gouvêa, T. DeGrand, P. de Jong, G. Dissertori, B.A. Dobrescu, M. D'Onofrio, M. Doser, M. Drees, H.K. Dreiner, D.A. Dwyer, P. Eerola, S. Eidelman, J. Ellis, J. Erler, V.V. Ezhela, W. Fetscher, B.D. Fields, R. Firestone, B. Foster, A. Freitas, H. Gallagher, L. Garren, H.-J. Gerber, G. Gerbier, T. Gershon, Y. Gershtein, T. Gherghetta, A.A. Godizov, M. Goodman, C. Grab, A.V. Gritsan, C. Grojean, D.E. Groom, M. Grünewald, A. Gurtu, T. Gutsche, H.E. Haber, C. Hanhart, S. Hashimoto, Y. Hayato, K.G. Hayes, A. Hebecker, S. Heinemeyer, B. Heltsley, J.J. Hernández-Rey, J. Hisano, A. Höcker, J. Holder, A. Holtkamp, T. Hyodo, K.D. Irwin, K.F. Johnson, M. Kado, M. Karliner, U.F. Katz, S.R. Klein, E. Klempt, R.V. Kowalewski, F. Krauss, M. Kreps, B. Krusche, Y.V. Kuyanov, Y. Kwon, O. Lahav, J. Laiho, J. Lesgourgues, A. Liddle, Z. Ligeti, C.-J. Lin, C. Lippmann, T.M. Liss, L. Littenberg, K.S. Lugovsky, S.B. Lugovsky, A. Lusiani, Y. Makida, F. Maltoni, T. Mannel, A.V. Manohar, W.J. Marciano, A.D. Martin, A. Masoni, J. Matthews, U.-G. Meißner, D. Milstead, R.E. Mitchell, K. Mönig, P. Molaro, F. Moortgat, M. Moskovic, H. Murayama, M. Narain, P. Nason, S. Navas, M. Neubert, P. Nevski, Y. Nir, K.A. Olive, S. Pagan Griso, J. Parsons, C. Patrignani, J.A. Peacock, M. Pennington, S.T. Petcov, V.A. Petrov, E. Pianori, A. Piepke, A. Pomarol, A. Quadt, J. Rademacker, G. Raffelt, B.N. Ratcliff, P. Richardson, A. Ringwald, S. Roesler, S. Rolli, A. Romaniouk, L.J. Rosenberg, J.L. Rosner, G. Rybka, R.A. Ryutin, C.T. Sachrajda, Y. Sakai, G.P. Salam, S. Sarkar, F. Sauli, O. Schneider, K. Scholberg, A.J. Schwartz, D. Scott, V. Sharma, S.R. Sharpe, T. Shutt, M. Silari, T. Sjöstrand, P. Skands, T. Skwarnicki, J.G. Smith, G.F. Smoot, S. Spanier, H. Spieler, C. Spiering, A. Stahl, S.L. Stone, T. Sumiyoshi, M.J. Syphers, K. Terashi, J. Terning, U. Thoma, R.S. Thorne, L. Tiator, M. Titov, N.P. Tkachenko, N.A. Törnqvist, D.R. Tovey, G. Valencia, R. Van de Water, N. Varelas, G. Venanzoni, L. Verde, M.G. Vincter, P. Vogel, A. Vogt, S.P. Wakely, W. Walkowiak, C.W. Walter, D. Wands, D.R. Ward, M.O. Wascko, G. Weiglein, D.H. Weinberg, E.J. Weinberg, M. White, L.R. Wiencke, S. Willocq, C.G. Wohl, J. Womersley, C.L. Woody, R.L. Workman, W.-M. Yao, G.P. Zeller, O.V. Zenin, R.-Y. Zhu, S.-L. Zhu, F. Zimmermann, P.A. Zyla, J. Anderson, L. Fuller, V.S. Lugovsky, P. Schaffner, Phys. Rev. D 98 (2018) 030001, http://dx.doi.org/10.1103/PhysRevD.98.030001, URL https://link.aps.org/doi/10.1103/PhysRevD.98.030001.